

# Tuning Electronic Structure in Layered Hybrid Perovskites with Organic Spacer Substitution

Joshua Leveille,<sup>\*,†,‡</sup> Claudine Katan,<sup>§</sup> Jacky Even,<sup>||</sup> Dibyajyoti Ghosh,<sup>‡,||</sup> Wanyi Nie,<sup>‡</sup> Aditya D. Mohite,<sup>⊥</sup> Sergei Tretiak,<sup>‡,||,¶</sup> André Schleife,<sup>‡,||,¶</sup> and Amanda J. Neukirch<sup>\*,‡,||</sup>

<sup>†</sup>Department of Materials Science and Engineering, University of Illinois at Urbana–Champaign, Urbana, Illinois 61801, United States

<sup>‡</sup>Los Alamos National Laboratory, Los Alamos, New Mexico 87545, United States

<sup>§</sup>Univ Rennes, ENSCR, INSA Rennes, CNRS, ISCR - UMR 6226, F-35000 Rennes, France

<sup>||</sup>Univ Rennes, INSA Rennes, CNRS, Institut FOTON - UMR 6082, F-35000 Rennes, France

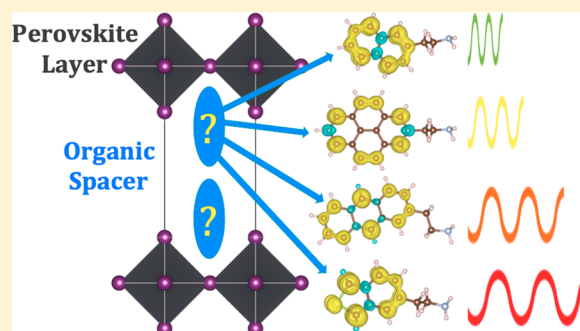
<sup>⊥</sup>Department of Chemical and Biomolecular Engineering, Rice University, Houston, Texas 77005, United States

<sup>¶</sup>Materials Research Laboratory, University of Illinois at Urbana–Champaign, Urbana, Illinois 61801, United States

<sup>#</sup>National Center for Supercomputing Applications, University of Illinois at Urbana–Champaign, Urbana, Illinois 61801, United States

## Supporting Information

**ABSTRACT:** Two-dimensional layered halide organic perovskites (LHOPs) are promising candidates for many optoelectronic applications due to their interesting tunable properties. They provide a unique opportunity to control energy and charge dynamics via the independent tunability of the energy levels within the perovskite and the organic spacer for various optoelectronic applications. In the perovskite layer alone, one can replace the Pb (Sn), the halide ( $X = \text{I}, \text{Br}, \text{Cl}$ ), the organic component, and the number of layers between the organic spacer layers. In addition, there are many possibilities for organic spacer layers between the perovskite layers, making it difficult for experimental methods to comprehensively explore such an extensive combinatorial space. Of



particular technological interest is alignment of electronic levels between the perovskite layer and the organic spacer layer, leading to desired transfer of energy or charge carriers between perovskite and organic components. For example, as band edge absorption is almost entirely attributed to the perovskite layer, one way to demonstrate energy transfer is to observe triplet emission from organic spacers. State-of-the-art computational chemistry tools can be used to predict the properties of many stoichiometries in search for LHOPs that have the most promising electronic-structure features. In this first-principles study, we survey a group of  $\pi$ -conjugated organic spacer candidates for use in triplet light-emitting LHOPs. Utilizing density functional theory (DFT) and time-dependent DFT, we calculate the first singlet ( $S_1$ ) and triplet ( $T_1$ ) excitation energy in the ground-state geometry and the first triplet excitation energy in the excited-triplet-state relaxed geometry ( $T_1^*$ ). By comparing these energies to the known lowest exciton energy level of  $\text{Pb}_x\text{X}_{3x+1}$  perovskite layers ( $X = \text{I}, \text{Br}, \text{Cl}$ ), we can identify organic spacer and perovskite layer pairings for possible transfer of Wannier excitons from the inorganic perovskite lattice to spin-triplet Frenkel excitons located on the organic cation. We successfully identify ten organic spacer candidates for possible pairing with perovskite layers of specific halide composition to achieve triplet light emission across the visible energy range. Molecular dynamics simulations predict that finite temperatures and perovskite environment have little influence on the average excitation energies of the two common organic spacers naphthylethylammonium (NEA) and phenylethylammonium (PEA). We find significant thermal broadening up to 0.5 eV of the optical excitation energies appearing due to finite temperature effects. The findings herein provide insights into alignment of electronic levels of the conjugated organic spacer with the layer.

**KEYWORDS:** Layered hybrid organic–inorganic perovskites, halide perovskite, organic spacer substitution, triplet light emission, exciton energy alignment, first-principles simulations

Two-dimensional (2D) layered hybrid metal–halide–organic perovskites (LHOPs) have come to the forefront of optoelectronic materials research due to their diverse and promising properties and applications. Most LHOPs assume a

**Received:** August 20, 2019

**Revised:** October 28, 2019

**Published:** November 1, 2019

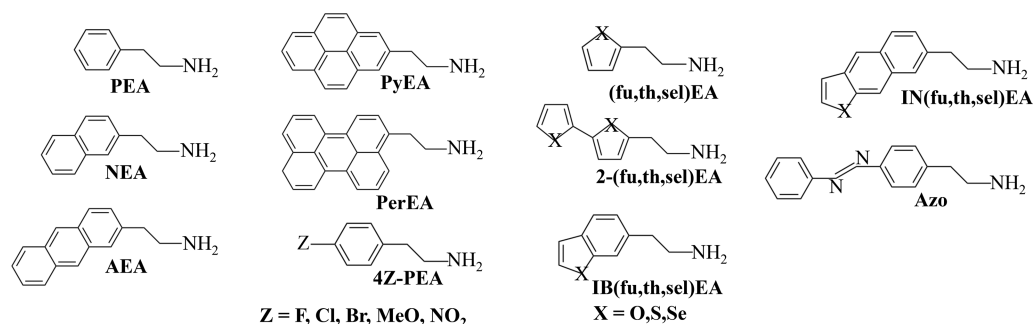


**Figure 1.** Organic spacer candidates considered in this work. Abbreviations include furan (fu), thiophene (th), selenophene (sel), isobenzol (IB), isonaphthyl (IN), 2-2'-bis (2), and azobenzene ethylammonia (Azo).

Ruddelston–Popper crystalline structure of  $A_2(\text{CH}_3\text{NH}_3)_{n-1}\text{M}_n\text{X}_{3n+1}$ , where  $A^{1+}$  is a large organic spacer,  $M^{2+}$  is a metal cation (usually Pb or Sn),  $X^{1-}$  is a halide anion, and  $n$  is the number of octahedra along the stacking axis in a single perovskite layer in stacking direction.<sup>1</sup> Stoichiometric design flexibility arises in the choice of perovskite layer thickness, metal–halide combination, and organic cation spacer.<sup>2</sup> Successes of LHOP materials designs include highly efficient solar cells,<sup>3</sup> tuned light-emitting diodes (LEDs),<sup>4–7</sup> and possible spintronics.<sup>8</sup> Recent studies have discovered that electronic and optical properties of the perovskite layer are heavily influenced by the choice of the organic spacer. The geometries of organic spacers strongly affect octahedra tilting in the perovskite layer and determine the band gap of the bulk material<sup>2</sup> as well as energies of surface states.<sup>9</sup> Furthermore, introducing more complex conjugated organic spacers has diversified the light-emitting properties of LHOPs,<sup>10</sup> leading to increased interest in band alignment and charge transfer between the perovskite and organic layers.<sup>11–14</sup> It is clear that the choice of organic cation is critical to the optical and electronic functionality of LHOP devices.

The electronic structures of 2D LHOPs are broadly tunable by the versatile alignment between the electronic levels of the perovskite and the organic spacer components. Depending on the degree of conjugation and polarity of the spacer moiety, one can precisely align desired electronic states including the perovskite levels and the singlet and triplet manifolds of the organic spacer layer. Knowledge of this provides materials scientists with a rich tool to control energy and charge dynamics via independent tunability of energy levels in the perovskite and organic components. Different applications require distinct electronic dynamics and transport, from separating p and n charge carrier channels between the perovskite and spacer layers, to storing excitons in the triplet states of the organic spacer layer and then reusing them as in thermally activated delayed fluorescence (TADF) emitters,<sup>15</sup> to attaining white-like broadband dual emission characteristics.<sup>16</sup> Of particular technological interest for many applications is engineering of the directed energy transfer between the perovskite layer and the organic spacer layer. Typically in these LHOP systems, the perovskite layer is the dominant component of band edge absorption.<sup>2,14,17–19</sup> Therefore, a way to demonstrate energy transfer would be to observe triplet emission from the organic spacer layer, which itself could be harnessed for several applications.

Markedly, over the past two decades, select LHOPs have demonstrated the ability to induce energy transfer from perovskite layer exciton states to low energy spin-triplet exciton states in the organic layer.<sup>20–22</sup> The fundamental differences of

the singlet–triplet exciton energy split between the perovskite and organic layers is critical to inducing such energy transfer processes. Within the perovskite layer, strong spin–orbit coupling and a high dielectric constant cause the differences between the singlet and triplet exchange integrals to be small and thus cause only little difference between singlet and triplet states. Consequently, these weakly bound and delocalized  $S_1$  and  $T_1$  Wannier–Mott excitons are hardly distinguishable in optical emission spectra.<sup>19,23,24</sup> In contrast, the collinear spin nature and small dielectric screening in the organic layer leads to a large difference in singlet and triplet exchange integrals, resulting in a drastic lowering of the  $T_1$  excitation energy compared to the  $S_1$  excitation energy.<sup>25</sup> The excitons in the organic layer are strongly bound Frenkel excitons. When the energy of the weakly bound exciton in the perovskite layer aligns with the energy  $T_1$  of the strongly bound exciton in the organic layer, charge transfer from the perovskite to the organic layer may occur.<sup>20–22</sup> After transfer, the  $T_1$  excitation energy in the organic relaxes to a lower  $T_1^*$  energy due to enhanced short-range atomic deformation, thus reaching optimal triplet molecular geometry. Phosphorescent photoemission is subsequently measured at the  $T_1^*$  excitation energy.<sup>26</sup> The choice and alignment of the exciton energy in the perovskite and  $T_1$  in the organic, and the photoemission energy  $T_1^*$  from the organic, are key design parameters leading to different options for LHOP photoemission materials. Subsequent light emission due to recombination from this triplet exciton is referred to as triplet emission. Electronic-structure methods provide a tool to better understand how to choose the various components within LHOPs to achieve desired material properties and optical response.

In this letter, we detail our first-principles survey of organic spacer triplet emission candidates for LHOPs. Each candidate consists of a conjugated chromophore attached to an ethylammonia tail ( $\text{C}_2\text{H}_4\text{-NH}_2$ ). The lowest spin-triplet excitation levels are calculated on the ground-state ( $S_0$ ) geometries to obtain the triplet energy  $T_1$  and the excited triplet geometry to obtain the triplet energy  $T_1^*$  in the  $\Delta$ SCF framework. The  $\Delta$ SCF approach has been shown to be a robust framework for predicting the lowest energy triplet state.<sup>27–30</sup> We also calculate the singlet and triplet excitation energies of several organic spacer candidates in clustered geometries and in the perovskite environment and predict similar excitation energies compared to the vacuum-relaxed molecular geometries. By means of molecular dynamics simulations for a few LHOP systems, we verify that our initial conclusions hold also under dynamic conditions but with significant thermally induced broadening of the excitation energies up to 0.5 eV. We are able to successfully identify promising triplet emission candidates for pairing with

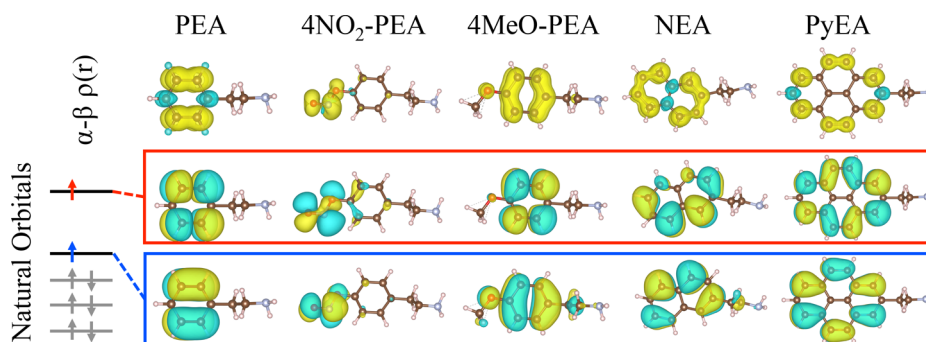


**Figure 2.** Spin density of the triplet state (top row) and natural orbitals of the open-shell states in selected organic spacer candidates.

known layered perovskite exciton levels to obtain possible triplet emission devices. We consider pairings with perovskite layers of varying layer thickness and halide stoichiometry, and the results herein provide the fundamental concepts for crafting materials with the desired response to various stimuli (light, field, charge injection).

Four classes of organic cation spacer molecules have been explored in this work (see molecular structures in Figure 1). The choices are motivated by organic spacers successfully used in LHOPs experimentally<sup>12,18,20–22</sup> and span diverse forms of conjugation (polycarbocyclic, heterocyclic, and electron rich/poor functionalization): First, five polycarbocyclic compounds with ethylammonium (EA) tails are studied. Among them are the basic phenylethylammonium (PEA), used extensively in LHOP synthesis, and the two-ring naphthylethylammonium (NEA), a different isomer which was investigated by Ema et al. and has shown promising application as a triplet emitter.<sup>22</sup> Three-ring anthrylethylammonium (AEA) has been explored less often but has promising low singlet and triplet energy states.<sup>20</sup> Four-ring pyrene–ethylammonium (PyEA) has only briefly been studied for its triplet emission properties,<sup>21</sup> whereas five-ring peryleneethylammonium (PerEA) has not been explored for its photoemission properties as spacers in LHOP systems.<sup>12</sup> The second class is functionalized PEA with the goal of adding electron-rich or -poor groups and additional linearly conjugated compounds. For electron-rich additions, halides F, Cl, and Br and NO<sub>2</sub> are added to the para position, opposite from the EA bonding site, on the phenyl group. Electron-poor methoxy (MeO) is attached to the same site. The third class are the heterocyclic compounds with carbon and chalcogen based rings. These include the pentacyclic furan–, thiophene–, and selenophene–ethylammonium (XEA, X = fu, th, sel) and their 2,2′ linked pentacyclic counterparts (2-XEA, X = fu, th, sel). Further, there are the fused ring compounds isobenzyl-(furan,thiophene,selenophene)–ethylammonium (IBXEA, X = fu, th, sel) and isonaphthyl(furan,thiophene,selenophene)–ethylammonium (INXEA, X = fu, th, sel). As a fourth class, we included azobenzene–ethylammonium to examine the effects of extended conjugation featuring the N–N double bond. In this work we refer to the atomic positions of the organic cation layers without the inorganic perovskite lattice, taken from a single unit cell of the experimental LHOP structures, as organic cluster geometries. PEA and NEA,<sup>18</sup> and PyOPA<sup>12</sup> clusters are investigated and initialized from atomic structures determined experimentally.

The predicted  $T_1$  and  $T_1^*$  energies of organic spacer candidates calculated by the  $\Delta$ SCF approach (see Computational Methods) span the visible and near-UV energy range (see Table S1 in the Supporting Information). Our calculations are in

agreement with available experimental data. For the most simple conjugated spacer, PEA, we compute  $T_1$  of 4.43 eV and  $T_1^*$  of 3.77 eV by using B3LYP. Since benzene is identical to the phenyl group in PEA we use it for comparison here, in the absence of PEA experimental data. This is further justified by the good agreement of  $\Delta$ SCF results for benzene,  $T_1^* = 3.88$  eV, and PEA as well as the good agreement between  $\Delta$ SCF and phosphorescence emission data of 3.40–3.60 eV.<sup>31</sup> The lowest phosphorescence emission energy  $T_1^*$  is predicted for NEA and PyEA, within 0.2 eV of the experimental NEA–PbBr<sub>4</sub><sup>22</sup> isomer and PyEA–PbI<sub>4</sub>.<sup>21</sup> Furthermore, the  $\Delta$ SCF model also predicts the  $T_1$  excitation energies of fuEA and thEA to within 100 meV of experimental results.<sup>32</sup> Given such good agreement, the  $\Delta$ SCF model can be used to make predictions on a number of other organic spacer candidates. We note that while this agreement is encouraging, these data were computed for vacuum-optimized isolated molecules. It is, thus, important to check what influence geometric and thermal effects have on these results, which will be discussed later.

We further analyze spatial localization of triplet excitations using the difference between up and down spin densities and complementary natural orbitals corresponding to unpaired electrons forming the triplet state. These orbitals are calculated as eigenfunctions of an open-shell ground-state density matrix of the molecule using the NBO (natural bond orbital) package<sup>33</sup> built into the Gaussian suite. We further refer the reader to a review<sup>34</sup> discussing various flavors of the natural orbital analysis in molecular systems. Both spin densities differences and natural orbitals are visualized for selected organic spacer candidates in Figure 2. It is found for all candidate spacers that the spin density difference is dispersed around the  $\pi$ -conjugated bonds of organic rings or on the nontail functional group. None of the cases studied here exhibits significant spin density difference localized on the EA tail. The natural orbitals for the two spins of the triplet configuration are generally localized in the same fashion. This indicates that orbitals delocalized over the conjugated rings or localized on the nontail functional group are the main participants in triplet excitations, while the nonconjugated tails provide little contributions.

Unlike other conjugated ring spacer candidates considered, the triplet excitation on 4NO<sub>2</sub>–PEA is localized near the bonds of the NO<sub>2</sub> as opposed to the conjugated ring. This removal of the excitation from the PEA ring causes 4NO<sub>2</sub>–PEA to exhibit a much lower  $T_1$  energy of 2.29 eV compared to the other functionalized PEA candidates (4.05–4.59 eV). This predicted  $T_1$  energy of 4NO<sub>2</sub>–PEA is in good agreement with the experimental  $T_1$  energy of NO<sub>2</sub> of 2.35 eV.<sup>35</sup> The origin of the lowered excitation energy is the conjugated bond series of O–N=O. The localization of the spin density, predicted at the

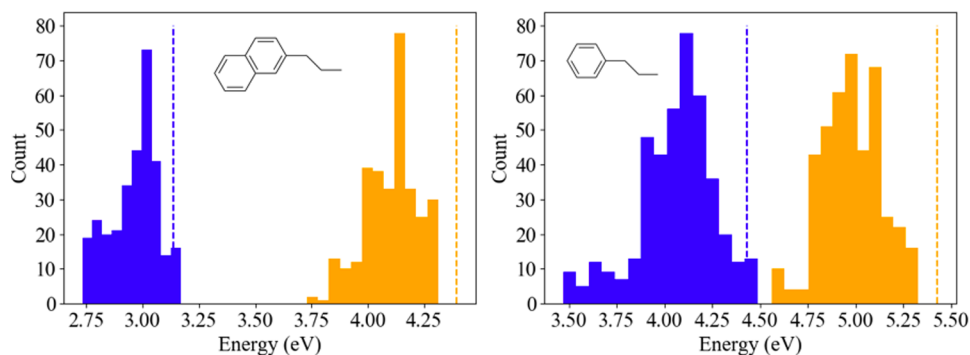


**Figure 3.** Histograms of  $\Delta$ SCF  $T_1$  (blue) and TDDFT  $S_1$  (orange) energies calculated on MD molecular conformations of NEA in NEA–PbI<sub>4</sub> (left) and PEA in PEA–PbI<sub>4</sub> (right). The vertical dashed line indicates the result for geometries optimized in vacuum for  $S_1$  (orange) and  $T_1$  (blue).

density functional level of theory, is validated for this case and confirmed by performing second order Møller–Plesset perturbation theory (MP2) calculations.<sup>36,37</sup> 4NO<sub>2</sub>–PEA highlights the possibility of conjugated compounds as alternative to ring structures for lowering the triplet energy level.

After calculating the excitation energies of organic spacer candidates in the gas phase, we move on to predict the excitation energies of clusters of organic spacers without the perovskite layer, in the geometries determined by X-ray diffraction experiments.<sup>12,18</sup> The geometries and orientation of individual organic molecules in LHOP crystals differ from that of isolated molecules due to interactions with each other and the perovskite layers. Du et al. examined PEA, PMA, NEA, and NMA organic spacers in Pb(I,Br,Cl)<sub>4</sub> systems and found varying behavior of tail geometries and penetration depth of the ammonium group into the perovskite octahedra layer.<sup>18</sup> One uniform characteristic of the conjugated ring organic spacers in the  $\langle 100 \rangle$  oriented class of LHOPs is the curling of the tail relative to the geometries of isolated molecules in vacuum. For example, the primary carbon of the naphthyl ring ( $C_1$ ) in NEA in the EA in the vacuum-relaxed geometry is 3.8 Å away from the nitrogen of the EA tail. In the perovskite environment, the tail curls back, resulting in the nitrogen moving closer to the carbon rings with a  $C_1$ –N distance of 3.02 Å in NEA–PbI<sub>4</sub>.<sup>18</sup> Smaller conjugated groups like PEA tend to arrange parallel to the perovskite layer while larger chromophores begin to tilt to a perpendicular position. Direct face-to-face  $\pi$ -stacking is not present in the organic layers considered in this study. Instead, the conjugated rings tend to arrange edge-to-face, a formation that is favorable to template the perovskite network.<sup>12</sup> Given these fundamental differences between perovskite and isolated geometries, it is important to understand how excitation spectra of organic spacer candidates change in the perovskite environment.

To this end, we examine how excitation energies of clusters of organic molecules PEA, NEA, and PyOPA in their experimental geometries differ compared to their isolated counterparts calculated in the gas phase. The clusters are taken as isolated layers from the unit cell, are nonperiodic, and consist of 4, 8, and 4 molecular species of PEA, NEA, and PyOPA, respectively. Figure S1c,d in the Supporting Information shows the simulated atomic structures for the NEA and PyOPA cluster, respectively. These organic compounds are chosen by available experimental atomic structures of layered perovskites in which they are the spacer. While PEA is unlikely to be a triplet emission candidate, NEA and PyEA (or PyOPA) show great potential due to their low  $T_1$  energies. PEA and NEA layer geometries of four and eight molecules, respectively, are taken from ref 18, and pyrene-

based organic layer geometries with OPA tails are taken from ref 12. First, no relaxations are performed on C, N, and O atoms, but since H atoms are not present in the XRD data, their positions are relaxed around the experimentally known atomic positions. Below we also test the effects of tail geometry by relaxing O, N, and C atoms, while keeping the tails fixed. We also note that one H atom is omitted from each NH<sub>3</sub><sup>+</sup> group to simulate neutral layers. This does not introduce detrimental effects on the geometries, since the tails are kept fixed.

The  $T_1$  energies calculated via the  $\Delta$ SCF method using the B3LYP XC functional for the organic spacer layer geometry without the perovskite layer, taken from experimental data of PEA ( $T_1 = 4.0$  eV) and PyOPA ( $T_1 = 2.35$  eV), are predicted within 0.5 eV of the vacuum-relaxed molecules of PEA ( $T_1 = 4.43$  eV) and PyEA ( $T_1 = 2.43$  eV). In contrast, the NEA experimental organic layer geometry ( $T_1 = 2.26$  eV) is predicted to have a  $\approx 0.96$  eV decrease in excitation energies compared to the isolated NEA molecule relaxed in vacuum ( $T_1 = 3.14$  eV). The source of this discrepancy lies with the molecular geometry differences where the experimental C–C bond lengths on the conjugated ring vary between 1.29 and 1.51 Å, whereas the isolated molecule has a smaller variation of 1.36–1.42 Å. It is worth noting that X-ray diffraction measurements do not pinpoint well the positions of light atoms such as carbon,<sup>38</sup> and therefore some variation in experimentally measured C–C bond lengths and atomic positions is to be expected. Finite temperature can induce additional variation in the molecular structure of spacers and, consequently, spacer excitation energies. Other crystallographic measurements of NEA and NMA (naphthal–methylammonium) structures have observed a C–C bond length range in the naphthal ring between 1.34 and 1.43 Å in NEA–CuCl<sub>4</sub><sup>39</sup> and NMA–SnI<sub>4</sub>.<sup>40</sup> This is very similar to the range found here for the isolated structures. Nonetheless it needs to be clarified (i) how the curled tail geometry influences the conjugated rings and (ii) how the periodic potential of the perovskite and other conjugated rings affects the variance of the chromophore geometry.

To further test the effects of tail geometry on the predicted  $T_1$  energies of organic candidates, a second set of calculations are performed where tail geometries are kept fixed at experimental geometries<sup>12,18</sup> while the conjugated rings are optimized. This test serves to determine if the bent tail significantly changes the orbital nature on the conjugated ring, thus changing the excitation spectrum. The resulting ring-relaxed B3LYP  $\Delta$ SCF  $T_1$  energies for the PEA cluster ( $T_1 = 4.42$  eV), NEA cluster ( $T_1 = 3.07$  eV), and PyOPA cluster ( $T_1 = 2.35$  eV) are predicted within 0.15 eV compared to the respective energies computed

for isolated geometries. We find that tail curling alone does not strongly affect the excitation spectrum of these molecules and does not change the spin density of the molecule, which remains localized on the ring (see Figure 2). Therefore, differences in the excitation energies calculated for isolated geometries and experimental structures, must originate from distinct conjugated ring geometries. This might be explained by the difficulties of pinpointing the precise position of light atoms, such as carbon, in XRD when heavy atoms, such as lead, are present in the system.

Using *ab initio* molecular dynamics (AIMD) simulations we further explore how the excitation energies of the organic spacer embedded in the perovskite layers, at finite temperature, differ from those relaxed in a vacuum. To this end, atomic geometries for PEA–PbI<sub>4</sub> and NEA–PbI<sub>4</sub> are initialized from atomic positions determined by XRD measurements by Du et al.<sup>18</sup> Prior to performing AIMD, we calculate the S<sub>1</sub> and T<sub>1</sub> energies of each unique crystalline organic PEA and NEA in these experimental geometries using TDDFT for S<sub>1</sub> and  $\Delta$ SCF for T<sub>1</sub> excitation energies. We find that the calculated T<sub>1</sub> energy of PEA remains in a narrow range between 4.43 and 4.46 eV for the individual spacer molecule geometries in the unit cell taken from the experimental XRD data. In contrast, the calculated T<sub>1</sub> energies of the NEA molecules vary between 2.23 and 3.26 eV, warranting further investigation by AIMD as discussed next.

AIMD results demonstrate that the excitation energies of PEA and NEA in the PbI<sub>4</sub> LHOP environment experience a broadening as a consequence of thermal fluctuations in the molecular geometries. Table S2 in the Supporting Information lists the explicit results, and Figure 3 shows the distributions of S<sub>1</sub> and T<sub>1</sub> excitation energies calculated across postequilibrium molecular conformations from AIMD. The average excitation energies for the different postequilibrium MD geometries are noticeably lower, compared to those of their isolated vacuum-relaxed counterparts. This results from a combination of longer average bond lengths in MD compared to XRD as well as complex torsion and bending in the NEA and PEA. The standard deviation in excitation energies lies between 0.11 and 0.20 eV, with the highest attributed to the T<sub>1</sub> excitation in PEA. The C–C bond lengths show high variability in PEA and NEA. For PEA, the simulated C–C variation exceeds the C–C bond length variations observed in XRD (1.39–1.41 Å). Alternatively, the variation in NEA bond length in the AIMD simulations remains lower compared to the XRD results. This explains why the T<sub>1</sub> energies calculated in the XRD PEA conformation fall within a narrow range whereas geometries sampled from AIMD show a higher variation. Overall, the findings herein demonstrate the importance of finite temperature dynamics on the broadening of S<sub>1</sub> and T<sub>1</sub> excitation energies of organic spacer candidates in LHOPs. As good agreement is observed between  $\bar{T}_1$  obtained from AIMD and T<sub>1</sub> calculated from vacuum-relaxed simulations, the latter results can be used for first-principles materials design of LHOPs for applications requiring specific alignments of electronic features.

Thus, from our analysis of the calculated excitation energies we identify multiple organic spacer candidates with low lying triplet states in Pb-based LHOPs with a variety of halides and number of perovskite layers (see Table 1 and Figure 4). The first major design consideration is the relative T<sub>1</sub> excitation energy of the organic spacer to the lowest excitation energy of the perovskite (with number of perovskite octahedra layers *n* = 1, 2, 3, etc.) E<sub>x</sub>. As previously discussed, the lowest triplet and singlet excitation energies in the perovskite layer are nearly indis-

**Table 1. Suggested Pairings of Organic Spacers with Perovskite Layers of Varying Halide and Layer Compositions<sup>a</sup>**

perovskite	org spacer	energy alignment (eV)
PbI <sub>4</sub> ( <i>n</i> = 1)	PyEA	2.50:2.43:2.10
	AEA	2.50:2.17:1.75
	IBselEA	2.50:2.17:1.77
	4NO <sub>2</sub> –PEA	2.50:2.29:0.68
Pb <sub>2</sub> I <sub>7</sub> ( <i>n</i> = 2)	PerEA	2.15:1.80:1.50
	Azo	2.15:1.95:1.25
PbBr <sub>4</sub> ( <i>n</i> = 1)	NEA	3.20:3.14:2.67
	2fuEA	3.20:3.14:2.40
PbCl <sub>4</sub> ( <i>n</i> = 1)	thEA	3.70:3.69:3.02
	selEA	3.70:3.57:2.93

<sup>a</sup>The energy alignment shows the perovskite exciton level E<sub>x</sub>, the organic triplet level in the ground-state geometry T<sub>1</sub> (charge transfer energy), and the organic triplet level in the excited-state geometry T<sub>1</sub><sup>\*</sup> (triplet emission energy), i.e., E<sub>x</sub>:T<sub>1</sub>:T<sub>1</sub><sup>\*</sup> (in eV).

tinguishable,<sup>23,24</sup> and thus we generate energy alignments with the lowest optical excitation peak energy in the perovskite E<sub>x</sub> from experimental data. When T<sub>1</sub> is less than but close to E<sub>x</sub>, strongly bound exciton energy transfer can be initiated from the perovskite to the organic. Once this transfer occurs, the organic spacer relaxes in the excited state, leading to a new T<sub>1</sub><sup>\*</sup> emission energy, which is the lowest energy phosphorescence peak. In the following, energy pairings will be given in E<sub>x</sub>:T<sub>1</sub>:T<sub>1</sub><sup>\*</sup> notation. Starting with single-layer PbCl<sub>4</sub>, the two optimal pairings are thEA–PbCl<sub>4</sub> and selEA–PbCl<sub>4</sub> with energy alignments of 3.7:3.69:3.02 and 3.7:3.57:2.93 eV, respectively. These LHOPs could produce a violet or indigo phosphorescence spectrum with a lowest emission wavelength of  $\approx$ 400 nm. As the functionalized PEA T<sub>1</sub> tends to be higher than 3.7 eV, thEA and selEA seem to be the only viable options for pairing with *n* = 1 PbCl<sub>4</sub> found in our work. The lowest exciton energy level of single-layer *n* = 1 PbCl<sub>4</sub> are referenced from Du et al.<sup>18</sup>

For *n* = 1 PbBr<sub>4</sub> perovskite layers, we also identify two promising organic spacer pairings: The optimal pairing is NEA–PbBr<sub>4</sub>, with an energy alignment of 3.20:3.14:2.67 eV. This first-principles prediction is supported by experimental evidence of highly efficient energy transfer from PbBr<sub>4</sub> to the triplet state of a NEA isomer by Ema et al.<sup>22</sup> They observe this process in a variety of naphthyl-based PbI<sub>4</sub> systems, encouraging further studies of these. Another possible pairing is 2-fuEA–PbBr<sub>4</sub>, which has an energy alignment of 3.20:2.91:2.40 eV and could exhibit triplet emission at 516 nm, corresponding to a green light. The lowest exciton energy level of single-layer *n* = 1 PbBr<sub>4</sub> is referenced from Du et al.<sup>18</sup>

The highest number of promising pairings of organic spacers for triplet emission occurs with *n* = 1 PbI<sub>4</sub> and *n* = 2 Pb<sub>2</sub>I<sub>7</sub>. The most obvious pairing for *n* = 1 PbI<sub>4</sub> is PyEA–PbI<sub>4</sub> with an energy alignment of 2.5:2.43:2.10 eV. This material would show triplet emission of yellow/orange light, which has been experimentally verified by Braun et al.<sup>21</sup> Another possibility is AEA–PbI<sub>4</sub> for an alignment of 2.5:2.17:1.75 eV, leading to red light triplet emission. Interestingly, AEA spacers in layered perovskites have rarely been explored for their light-emitting properties, despite promising exciton energy level alignment. A similar energy alignment of 2.5:2.17:1.77 eV and potential red light triplet emission can be achieved by the pairing IBselEA–PbI<sub>4</sub>. Finally, 4NO<sub>2</sub>–PEA is predicted to have an alignment with *n* = 1 PbI<sub>4</sub> of 2.5:2.29:0.68 eV, indicating potential infrared triplet emission in

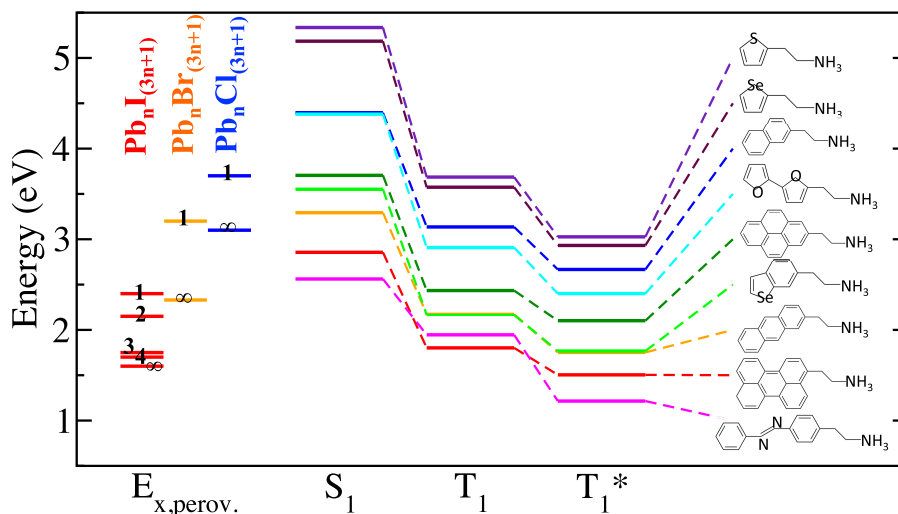


**Figure 4.** Alignment between perovskite  $E_x$  exciton levels, organic triplet  $T_1$  excitation energies, and organic  $T_1^*$  excited-state geometry emission energies for a select subset of examined organic spacers. Perovskite exciton energy levels are referenced from previous experimental data.<sup>18,41</sup>

4NO<sub>2</sub>–PEA–PbI<sub>4</sub>. As previously discussed, a low  $T_1^*$  in 4NO<sub>2</sub>–PEA is attributed to the localization of the triplet excitation on the NO<sub>2</sub> functional group (Figure 2).

Two-layer  $n = 2$  Pb<sub>2</sub>I<sub>7</sub> is also predicted to have spacer candidates for deep red triplet emission: The first two are PerEA and AzEA, with alignments of 2.15:1.80:1.50 and 2.15:2.08:1.75 eV, respectively. The pairing with PerEA should be given careful attention, given the recent inclusion of PerEA in layered perovskite by Passarelli et al.<sup>12</sup> Finally, Azo can be paired with  $n = 2$  Pb<sub>2</sub>I<sub>7</sub> for an alignment of 2.15:1.95:1.25 eV, giving yet another spacer for possible infrared triplet emission. The lowest exciton energy levels of one, two, three, four, and infinite (3D) layered Pb<sub>n</sub>I<sub>4n-1</sub>, as discussed here and shown in Figure 4, are references from Blancon et al.<sup>41</sup>

In addition to these, multiple of the considered compounds have nonideal alignment with the known perovskite layer absorption edges but should not be entirely discounted. Compounds with  $T_1$  energies between 2.5 and 2.8 eV are mismatched with  $n = 1$  PbI<sub>4</sub> and are unlikely to induce energy transfer from  $n = 1$  PbBr<sub>4</sub>, including 2-(th,sel)EA and IN(fu,th,sel)EA. However, little is currently known about the perovskite exciton levels of  $n = 2$  Pb<sub>2</sub>Br<sub>7</sub> and it is possible that alignment is better in this case. Given experimental evidence from  $n = 2$  Pb<sub>2</sub>I<sub>7</sub>,<sup>6</sup> it is likely that  $n = 2$  Pb<sub>2</sub>Br<sub>7</sub> would demonstrate a  $E_x$  level between 3.2 eV for  $n = 1$  PbBr<sub>4</sub> and 2.4 eV for  $n = \infty$  PbBr<sub>3</sub>. Thus, some of the aforementioned nonideal compounds for pairing with PbI<sub>4</sub> or PbBr<sub>4</sub> could provide an ideal pairing with  $n = 2$  Pb<sub>2</sub>Br<sub>7</sub>. Experimental observation of  $E_x$  from  $n = 2$  Pb<sub>2</sub>Br<sub>7</sub> would be required to make a definite claim. In contrast, the single ring compounds and {Br, Cl, F, MeO}-functionalized PEA all have high  $T_1$  compared to  $E_x$  of  $n = 1$  PbCl<sub>4</sub> and, therefore, are highly unlikely to induce excitation transfer.

A brief discussion on possible exciton transfer mechanisms, though not simulated in this work, is useful. It is important to note that the  $S_1$  and  $T_1$  states in both three-dimensional HOPs and two-dimensional LHOPs are nearly indistinguishable, differing by no more than 25 meV.<sup>23,42</sup> This can be attributed to the strong spin–orbit coupling, where  $J = S + L$  is a good quantum number for the Wannier-type exciton generated in the perovskite upon optical absorption or charge injection. The influence of spin–orbit coupling is much weaker in the organic layer, where the enhanced Coulomb exchange strongly splits the

$S_1$  and  $T_1$  energies, resulting in strongly bound Frenkel excitons. Thus, the energy transfer involves a transfer of the mixed singlet and triplet Wannier–Mott exciton in the strongly spin–orbit coupled perovskite layer to the triplet Frenkel exciton in the organic layer. The first, and most likely, possible charge transfer mechanism is the Dexter mechanism,<sup>43</sup> hypothesized by Ema et al. as the source of triplet emission in an isomer of NEA<sub>2</sub>–PbBr<sub>4</sub>.<sup>22</sup> Dexter charge transfer requires a significant orbital overlap between the organic and perovskite species and is highly dependent on individual atomic structures of LHOP systems. Ema et al. noted that the length of the organic cation tail strongly influences the triplet exciton transfer rate, suggesting that the Dexter mechanism is at play.<sup>22</sup> Another possible mechanism would be a charge transfer through a series of excimer and exciplex intermediate states,<sup>44</sup> though no studies have been performed on this concerning LHOPs to the knowledge of the authors. Finally, Förster resonance energy transfer (FRET) could be induced by dipole–dipole interaction, leading to excitation in the organic spacer layer via nonradiative de-excitation in the perovskite layer.<sup>45</sup> Notably, while FRET is less sensitive to the distance between donor and acceptor species compared, for example, to the Dexter mechanism, vanishing transition dipole moments of  $T_1$  states of organic molecules effectively rule out this scenario. However, the spin–orbit coupling in organics may be enhanced by the presence of perovskites. This may potentially enable a weak FRET channel and improve triplet emission compared to that in the isolated molecules. Further investigation on the energy and charge transfer mechanisms between the perovskite layer and the organic spacer will thus be an important next step to designing functional LHOPs.

In conclusion, we use electronic-structure calculations to predict multiple viable pairings of organic spacer candidates with single perovskite layers, to facilitate design of LHOPs with desired energy level alignments. These pairings may achieve potential triplet emission across the visible spectral range, offering potential solutions for tuned light emission applications. We carefully verified that our predictions remain consistent even when tail geometries are altered and organic candidates are placed into their clustered LHOP geometries. Finally, finite temperature dynamics of organic spacers in the perovskite crystal, as simulated by ab initio molecular dynamics, result in a

broadening of excitation energies slightly below the results obtained for isolated geometries. This thermal broadening of the excitation energies provides an important consideration for future theoretical and experimental work in designing light emitting LHOP devices. Altogether our computational predictions demonstrate that electronic structure of LHOPs paired with conjugated organic spacers is extremely tunable, which suggests broad variability and control over dynamics of energy and charge carriers. In particular, light-emitting applications involving LHOPs is a promising field of research and should be further investigated to discover potential next generation, wavelength tuned, highly efficient light sources.

**Computational Methods.** First-principles simulations for the singlet excitation, triplet excitation, and the energy gap between the highest occupied and lowest unoccupied molecular orbitals (HOMO–LUMO gap) based on  $\Delta$ SCF and time-dependent density functional theory (TDDFT) are performed in this work.

Ground-state closed- and open-shell DFT calculations of spin singlet and triplet excitations are conducted using the Gaussian code.<sup>46</sup> These use occupation number and spin orientation constraints to enforce the total spin  $S$  to 0 or 1, respectively. As such, the pure spin states are eigenstates of the Kohn–Sham Hamiltonian. Charge densities and single-particle wave functions are calculated in a Gaussian 6-31G\* basis set on pruned ultrafine real space grids with 99 590 real space integration points around the atoms. For heavy Br ions, a LANL2DZ Gaussian basis set is tested and found to be comparable in accuracy to 6-31G\* (see Table S9 in the Supporting Information). For neutral molecules in vacuum, structural relaxations are performed in the singlet configuration with the B3LYP exchange–correlation functional.<sup>47</sup>

Triplet excitations are calculated using the  $\Delta$ SCF approach, due to its predictive power for the  $S_0$  geometry triplet and  $T_1^*$  geometry triplet energies. In addition,  $\Delta$ SCF avoids triplet instability errors that occur in TDDFT.<sup>29,30,48,49</sup> In TDDFT, the difference between singlet and triplet can become larger than the HOMO–LUMO gap,<sup>30</sup> forcing the triplet excitation energies to become excessively small or even negative in some cases. Sears et al.<sup>30</sup> point to the difference of the exchange contribution between singlet and triplet within a given exchange–correlation functional as the source of this triplet instability. The  $\Delta$ SCF approach avoids this issue, since it relies on the difference between total Kohn–Sham energies of singlet and triplet states. Lowest energy singlet excitations are calculated within the TDDFT framework in the frequency domain, from the solution of the Casida equation.<sup>50</sup> TDDFT has been shown to provide reliable singlet excitation energies in organic molecules for charge transfer and optical excitations.<sup>51</sup> While  $T_1$  excitation energies are also calculated by TDDFT (see Tables S3 through S12 in the Supporting Information), they underestimate the excitation energies due to the aforementioned triplet instability<sup>48</sup> and are thus not discussed in the main text. Excitation energies are separately calculated using HSE,<sup>52</sup> B3LYP,<sup>47</sup> and CAM-B3LYP<sup>53</sup> exchange–correlation functionals within  $\Delta$ SCF and TDDFT. It is found that the introduction of solvent effects of water using the polarization continuum model<sup>54</sup> does not change the predicted  $S_1$  and  $T_1$  energies significantly (see Table S13 of the Supporting Information). CAM-B3LYP is used to compare the excitation energies of charged ( $\text{NH}_3^+$ -terminated) and uncharged ( $\text{NH}_2$ -terminated) species, due to it is improved handling of long-range exchange under charged conditions. The results are comparable within tens of millielectronvolts (see

Tables S8 through S12 in the Supporting Information). As tail charge is inconsequential to the chromophore excitation energies and since B3LYP better handles the triplet instability compared to CAM-B3LYP and HSE in extensively conjugated systems, B3LYP results are presented in this letter. However, for natural bonding orbital analysis and to predict changes in natural atomic charges when going from tails with  $\text{NH}_2$  to  $\text{NH}_3^+$ , we use CAM-B3LYP due to its ability to better handle excitations in the charged state. All these simulations are done on geometries relaxed in the vacuum, and detailed results are tabulated in Tables S3 through S12 of the Supporting Information.

To understand how finite temperature in the perovskite environment affects molecular geometry and singlet and triplet excitation energies, we run ab initio molecular dynamics simulations. These are performed using the VASP code,<sup>55–58</sup> the PAW method, and the PBE exchange–correlation functional<sup>59</sup> with Grimme-D2 van der Waals corrections<sup>60</sup> in the NVT ensemble with a Nose–Hoover thermostat at 300 K. The simulations are initialized with experimental geometries<sup>18</sup> and after thermal equilibrium is reached, molecular geometries at each time step are used for simulating the singlet and triplet excitation energies using the Gaussian code.

## ■ ASSOCIATED CONTENT

### Supporting Information

The Supporting Information is available free of charge on the ACS Publications website at DOI: 10.1021/acs.nanolett.9b03427.

Explicit calculated data for singlet  $S_1$  and triplet  $T_1$  and triplet emission  $T_1^*$  energies for all investigated compounds along with a supplemental figure showing the simulated organic clusters of NEA and PyOPA (PDF)

## ■ AUTHOR INFORMATION

### Corresponding Authors

\*leveill2@illinois.edu.

\*ajneukirch@lanl.gov.

### ORCID

Joshua Leveille: 0000-0003-2393-3973

Claudine Katan: 0000-0002-2017-5823

Jacky Even: 0000-0002-4607-3390

Dibyajyoti Ghosh: 0000-0002-3640-7537

Sergei Tretiak: 0000-0001-5547-3647

André Schleife: 0000-0003-0496-8214

Amanda J. Neukirch: 0000-0002-6583-0086

### Notes

The authors declare no competing financial interest.

## ■ ACKNOWLEDGMENTS

The work at Los Alamos National Laboratory (LANL) was supported by the LANL Directed Research and Development Funds (LDRD). This work was conducted, in part, at the Center for Nonlinear Studies and the Center for Integrated Nanotechnologies, U.S. Department of Energy (DOE), Office of Basic Energy Sciences user facility at LANL. This research used resources provided by the LANL Institutional Computing (IC) Program. LANL is operated by Triad National Security, LLC, for the National Nuclear Security Administration of the U.S. Department of Energy (Contract No. 89233218NCA000001). Work performed at UIUC was supported by the National Science Foundation under Grant No. DMR-1555153. This

research is partially supported by the Blue Waters sustained-petascale computing project, which is supported by the National Science Foundation (awards OCI-0725070 and ACI-1238993) and the state of Illinois. Blue Waters is a joint effort of the University of Illinois at Urbana-Champaign and its National Center for Super Computing Applications. J.E. acknowledges the Institut Universitaire de France. The work in France was supported by Agence Nationale pour la Recherche (TRANS-HYPERO projects). A.D.M. acknowledges funding from DOE-EERE 2022-1652 for support for this work.

## REFERENCES

- (1) Ruddlesden, S. N.; Popper, P. New compounds of the  $K_2NiF_4$  type. *Acta Crystallogr.* **1957**, *10*, 538–539.
- (2) Pedesseau, L.; Saponi, D.; Traore, B.; Robles, R.; Fang, H.-H.; Loi, M. A.; Tsai, H.; Nie, W.; Blancon, J.-C.; et al. Advances and Promises of Layered Halide Hybrid Perovskite Semiconductors. *ACS Nano* **2016**, *10*, 9776–9786.
- (3) Cho, K. T.; Grancini, G.; Lee, Y.; Oveisi, E.; Ryu, J.; Almora, O.; Tschumi, M.; Schouwink, P. A.; Seo, G.; Heo, S.; et al. Selective growth of layered perovskites for stable and efficient photovoltaics. *Energy Environ. Sci.* **2018**, *11*, 952–959.
- (4) Dohner, E. R.; Jaffe, A.; Bradshaw, L. R.; Karunadasa, H. I. Intrinsic White-Light Emission from Layered Hybrid Perovskites. *J. Am. Chem. Soc.* **2014**, *136*, 13154–13157.
- (5) Smith, M. D.; Karunadasa, H. I. White-Light Emission from Layered Halide Perovskites. *Acc. Chem. Res.* **2018**, *51*, 619–627.
- (6) Mao, L.; Ke, W.; Pedesseau, L.; Wu, Y.; Katan, C.; Even, J.; Wasielewski, M. R.; Stoumpos, C. C.; Kanatzidis, M. G. Hybrid Dion-Jacobson 2D Lead Iodide Perovskites. *J. Am. Chem. Soc.* **2018**, *140*, 3775–3783.
- (7) Tsai, H.; Nie, W.; Blancon, J.-C.; Stoumpos, C. C.; Soe, C. M. M.; Yoo, J.; Crochet, J.; Tretiak, S.; Even, J.; Sadhanala, A.; et al. Stable Light-Emitting Diodes Using Phase-Pure Ruddlesden-Popper Layered Perovskites. *Adv. Mater.* **2018**, *30*, 1704217.
- (8) Wang, J.; Zhang, C.; Liu, H.; McLaughlin, R.; Zhai, Y.; Vardeny, S. R.; Liu, X.; McGill, S.; Semenov, D.; Guo, H.; et al. Spin-optoelectronic devices based on hybrid organic-inorganic trihalide perovskites. *Nat. Commun.* **2019**, *10*, 129.
- (9) Kepenekian, M.; Traore, B.; Blancon, J.-C.; Pedesseau, L.; Tsai, H.; Nie, W.; Stoumpos, C. C.; Kanatzidis, M. G.; Even, J.; Mohite, A. D.; et al. Concept of Lattice Mismatch and Emergence of Surface States in Two-dimensional Hybrid Perovskite Quantum Wells. *Nano Lett.* **2018**, *18*, 5603–5609.
- (10) Smith, M. D.; Connor, B. A.; Karunadasa, H. I. Tuning the Luminescence of Layered Halide Perovskites. *Chem. Rev.* **2019**, *119*, 3104–3139.
- (11) Mitzi, D. B.; Chondroudis, K.; Kagan, C. R. Design, Structure, and Optical Properties of Organic-Inorganic Perovskites Containing an Oligothiophene Chromophore. *Inorg. Chem.* **1999**, *38*, 6246–6256.
- (12) Passarelli, J. V.; Fairfield, D. J.; Sather, N. A.; Hendricks, M. P.; Sai, H.; Stern, C. L.; Stupp, S. I. Enhanced Out-of-Plane Conductivity and Photovoltaic Performance in  $n = 1$  Layered Perovskites through Organic Cation Design. *J. Am. Chem. Soc.* **2018**, *140*, 7313–7323.
- (13) Traore, B.; Pedesseau, L.; Assam, L.; Che, X.; Blancon, J.-C.; Tsai, H.; Nie, W.; Stoumpos, C. C.; Kanatzidis, M. G.; Tretiak, S.; et al. Composite Nature of Layered Hybrid Perovskites: Assessment on Quantum and Dielectric Confinements and Band Alignment. *ACS Nano* **2018**, *12*, 3321–3332.
- (14) Katan, C.; Mercier, N.; Even, J. Quantum and Dielectric Confinement Effects in Lower-Dimensional Hybrid Perovskite Semiconductors. *Chem. Rev.* **2019**, *119*, 3140–3192.
- (15) Uoyama, H.; Goushi, K.; Shizu, K.; Nomura, H.; Adachi, C. Highly efficient organic light-emitting diodes from delayed fluorescence. *Nature* **2012**, *492*, 234–238.
- (16) Sheng, C. X.; Singh, S.; Gambetta, A.; Drori, T.; Tong, M.; Tretiak, S.; Vardeny, Z. V. Ultrafast intersystem-crossing in platinum containing  $\pi$ -conjugated polymers with tunable spin-orbit coupling. *Sci. Rep.* **2013**, *3*, 2653.
- (17) Gebhardt, J.; Kim, Y.; Rappe, A. M. Influence of the Dimensionality and Organic Cation on Crystal and Electronic Structure of Organometallic Halide Perovskites. *J. Phys. Chem. C* **2017**, *121*, 6569–6574.
- (18) Du, K.-z.; Tu, Q.; Zhang, X.; Han, Q.; Liu, J.; Zauscher, S.; Mitzi, D. B. Two-Dimensional Lead(II) Halide-Based Hybrid Perovskites Templated by Acene Alkylamines: Crystal Structures, Optical Properties, and Piezoelectricity. *Inorg. Chem.* **2017**, *56*, 9291–9302.
- (19) Leveille, J.; Katan, C.; Zhou, L.; Mohite, A. D.; Even, J.; Tretiak, S.; Schleife, A.; Neukirch, A. J. Influence of  $\pi$ -conjugated cations and halogen substitution on the optoelectronic and excitonic properties of layered hybrid perovskites. *Phys. Rev. Materials* **2018**, *2*, 105406.
- (20) Braun, M.; Tuffentsammer, W.; Wachtel, H.; Wolf, H. Tailoring of energy levels in lead chloride based layered perovskites and energy transfer between the organic and inorganic planes. *Chem. Phys. Lett.* **1999**, *303*, 157–164.
- (21) Braun, M.; Tuffentsammer, W.; Wachtel, H.; Wolf, H. Pyrene as emitting chromophore in organic-inorganic lead halide-based layered perovskites with different halides. *Chem. Phys. Lett.* **1999**, *307*, 373–378.
- (22) Ema, K.; Inomata, M.; Kato, Y.; Kunugita, H.; Era, M. Nearly Perfect Triplet-Triplet Energy Transfer from Wannier Excitons to Naphthalene in Organic-Inorganic Hybrid Quantum-Well Materials. *Phys. Rev. Lett.* **2008**, *100*, 257401.
- (23) Tamarat, P.; Bodnarchuk, M. I.; Trebbia, J.-B.; Erni, R.; Kovalenko, M. V.; Even, J.; Lounis, B. The ground exciton state of formamidinium lead bromide perovskite nanocrystals is a singlet dark state. *Nat. Mater.* **2019**, *18*, 717–724.
- (24) Thouin, F.; Valverde-Chávez, D. A.; Quarti, C.; Cortecchia, D.; Bargigia, I.; Beljonne, D.; Petrozza, A.; Silva, C.; Srimath Kandada, A. R. Phonon coherences reveal the polaronic character of excitons in two-dimensional lead halide perovskites. *Nat. Mater.* **2019**, *18*, 349–356.
- (25) Tanaka, K.; Takahashi, T.; Kondo, T.; Umeda, K.; Ema, K.; Umabayashi, T.; Asai, K.; Uchida, K.; Miura, N. Electronic and Excitonic Structures of Inorganic–Organic Perovskite-Type Quantum-Well Crystal (C<sub>4</sub>H<sub>9</sub>NH<sub>3</sub>)<sub>2</sub>PbBr<sub>4</sub>. *Jp J. Appl. Phys.* **2005**, *44*, S923–S932.
- (26) Jüstel, T.; Möller, S.; Winkler, H.; Adam, W. *Ullmann's Encyclopedia of Industrial Chemistry*; American Cancer Society, 2012.
- (27) Frank, I.; Hutter, J.; Marx, D.; Parrinello, M. Molecular dynamics in low-spin excited states. *J. Chem. Phys.* **1998**, *108*, 4060–4069.
- (28) Grimm, S.; Nonnenberg, C.; Frank, I. Restricted open-shell Kohn–Sham theory for  $\pi$ - $\pi^*$  transitions. I. Polyenes, cyanines, and protonated imines. *J. Chem. Phys.* **2003**, *119*, 11574–11584.
- (29) Gavnholt, J.; Olsen, T.; Engelund, M.; Schiøtz, J.  $\Delta$ self-consistent field method to obtain potential energy surfaces of excited molecules on surfaces. *Phys. Rev. B: Condens. Matter Mater. Phys.* **2008**, *78*, 075441.
- (30) Sears, J. S.; Koerzdoerfer, T.; Zhang, C.-R.; Brédas, J.-L. Communication: Orbital instabilities and triplet states from time-dependent density functional theory and long-range corrected functionals. *J. Chem. Phys.* **2011**, *135*, 151103.
- (31) Ishikawa, H.; Noyes, W. A. The Triplet State of Benzene. *J. Am. Chem. Soc.* **1962**, *84*, 1502–1503.
- (32) Flicker, W. M.; Mosher, O. A.; Kuppermann, A. Triplet states of furan, thiophene, and pyrrole. *Chem. Phys. Lett.* **1976**, *38*, 489–492.
- (33) Glendenning, E. D.; Badenhop, J. K.; Reed, A. E.; Carpenter, J. E.; Bohmann, J. A.; Morales, C. M.; Landis, C. R.; Weinhold, F. *NBO 6.0*; 2012.
- (34) Reed, A. E.; Curtiss, L. A.; Weinhold, F. Intermolecular interactions from a natural bond orbital, donor-acceptor viewpoint. *Chem. Rev.* **1988**, *88*, 899–926.
- (35) Hochstrasser, R. M.; Marchetti, A. P. Electronic, Vibrational, and Zeeman Spectra of Triplet NO<sub>2</sub>. *J. Chem. Phys.* **1969**, *50*, 1727–1736.
- (36) Möller, C.; Plesset, M. S. Note on an Approximation Treatment for Many-Electron Systems. *Phys. Rev.* **1934**, *46*, 618–622.
- (37) Head-Gordon, M.; Pople, J. A.; Frisch, M. J. MP2 energy evaluation by direct methods. *Chem. Phys. Lett.* **1988**, *153*, 503–506.

(38) Cullity, B.; Stock, S. *Elements of X-ray Diffraction*, third ed.; Prentice-Hall, 2001.

(39) Mande, H. M.; Ghalsasi, P. S.; Navamoney, A. Synthesis, structural and spectroscopic characterization of the thermochromic compounds  $A_2CuCl_4$ : [(Naphthyl ethylammonium) $2CuCl_4$ ]. *Polyhedron* **2015**, *91*, 141–149.

(40) Lemmerer, A. Phase transitions and structural motifs of inorganic-organic lead halide hybrids. *Ph.D. thesis*, University of the Witwatersrand, Johannesburg, 2008.

(41) Blancon, J.-C.; Tsai, H.; Nie, W.; Stoumpos, C. C.; Pedesseau, L.; Katan, C.; Kepenekian, M.; Soe, C. M. M.; Appavoo, K.; Sfeir, M. Y.; et al. Extremely efficient internal exciton dissociation through edge states in layered 2D perovskites. *Science* **2017**, *355*, 1288–1292.

(42) Ema, K.; Umeda, K.; Toda, M.; Yajima, C.; Arai, Y.; Kunugita, H.; Wolverson, D.; Davies, J. J. Huge exchange energy and fine structure of excitons in an organic-inorganic quantum well material. *Phys. Rev. B: Condens. Matter Mater. Phys.* **2006**, *73*, 241310.

(43) Dexter, D. L. A. Theory of Sensitized Luminescence in Solids. *J. Chem. Phys.* **1953**, *21*, 836–850.

(44) Yip, W. T.; Levy, D. H. Excimer/Exciplex Formation in van der Waals Dimers of Aromatic Molecules. *J. Phys. Chem.* **1996**, *100*, 11539–11545.

(45) Förster, T. Zwischenmolekulare Energiewanderung und Fluoreszenz. *Ann. Phys.* **1948**, *437*, 55–75.

(46) Frisch, M. J.; Trucks, G. W.; Schlegel, H. B.; Scuseria, G. E.; Robb, M. A.; Cheeseman, J. R.; Scalmani, G.; Barone, V.; Petersson, G. A.; Nakatsuji, H.; et al., *Gaussian 16*, Revision B.01; Gaussian Inc. Wallingford CT, 2016.

(47) Becke, A. D. Density-functional thermochemistry. III. The role of exact exchange. *J. Chem. Phys.* **1993**, *98*, 5648–5652.

(48) Peach, M. J. G.; Williamson, M. J.; Tozer, D. J. Influence of Triplet Instabilities in TDDFT. *J. Chem. Theory Comput.* **2011**, *7*, 3578–3585.

(49) Tozer, D. J.; Handy, N. C. On the determination of excitation energies using density functional theory. *Phys. Chem. Chem. Phys.* **2000**, *2*, 2117–2121.

(50) Casida, M.; Ipatov, A.; Cordova, F. In *Time-Dependent Density Functional Theory*; Marques, M. A., Ullrich, C. A., Nogueira, F., Rubio, A., Burke, K., Gross, E. K. U., Eds.; Springer: Berlin, Heidelberg, 2006; pp 243–257.

(51) Guido, C. A.; Knecht, S.; Kongsted, J.; Mennucci, B. Benchmarking Time-Dependent Density Functional Theory for Excited State Geometries of Organic Molecules in Gas-Phase and in Solution. *J. Chem. Theory Comput.* **2013**, *9*, 2209–2220.

(52) Heyd, J.; Scuseria, G. E.; Ernzerhof, M. Hybrid functionals based on a screened Coulomb potential. *J. Chem. Phys.* **2003**, *118*, 8207–8215.

(53) Yanai, T.; Tew, D. P.; Handy, N. C. A new hybrid exchange–correlation functional using the Coulomb-attenuating method (CAM-B3LYP). *Chem. Phys. Lett.* **2004**, *393*, 51–57.

(54) Tomasi, J.; Mennucci, B.; Cammi, R. Quantum Mechanical Continuum Solvation Models. *Chem. Rev.* **2005**, *105*, 2999–3094.

(55) Kresse, G.; Hafner, J. Ab Initio Molecular Dynamics for Liquid Metals. *Phys. Rev. B: Condens. Matter Mater. Phys.* **1993**, *47*, 558–561.

(56) Kresse, G.; Furthmüller, J. Efficiency of Ab-Initio Total Energy Calculations for Metals and Semiconductors Using a Plane-Wave Basis Set. *Comput. Mater. Sci.* **1996**, *6*, 15–50.

(57) Kresse, G.; Furthmüller, J. Efficient Iterative Schemes for Ab Initio Total-Energy Calculations Using a Plane-Wave Basis Set. *Phys. Rev. B: Condens. Matter Mater. Phys.* **1996**, *54*, 11169–11186.

(58) Kresse, G.; Joubert, D. From Ultrasoft Pseudopotentials to the Projector Augmented-Wave Method. *Phys. Rev. B: Condens. Matter Mater. Phys.* **1999**, *59*, 1758–1775.

(59) Perdew, J. P.; Burke, K.; Ernzerhof, M. Generalized Gradient Approximation Made Simple. *Phys. Rev. Lett.* **1996**, *77*, 3865–3868.

(60) Grimme, S. Semiempirical GGA-type density functional constructed with a long-range dispersion correction. *J. Comput. Chem.* **2006**, *27*, 1787–1799.